Opto-Electronic Advances

CN 51–1781/TN ISSN 2096–4579 (Print) ISSN 2097–3993 (Online)

An inversely designed integrated spectrometer with reconfigurable performance and ultra-low power consumption

Ang Li, Yifan Wu, Chang Wang, Feixia Bao, Zongyin Yang and Shilong Pan

Citation: Li A, Wu YF, Wang C, et al. An inversely designed integrated spectrometer with reconfigurable performance and ultra-low power consumption. *Opto-Electron Adv* **7**, 240099(2024).

https://doi.org/10.29026/oea.2024.240099

Received: 28 April 2024; Accepted: 3 June 2024; Published online: 17 July 2024

Opto-Electronic Advances

Article

August 2024, Vol. 7, No. 8

DOI: 10.29026/oea.2024.240099

An inversely designed integrated spectrometer with reconfigurable performance and ultra-low power consumption

Ang Li[1,2], Yifan Wu[1], Chang Wang[1], Feixia Bao[1], Zongyin Yang[3]* and Shilong Pan[1]*

Despite the pressing demand for integrated spectrometers, a solution that deliver high-performance while being practically operated is still missing. Furthermore, current integrated spectrometers lack reconfigurability in their performance, which is highly desirable for dynamic working scenarios. This study presents a viable solution by demonstrating a user-friendly, reconfigurable spectrometer on silicon. At the core of this innovative spectrometer is a programmable photonic circuit capable of exhibiting diverse spectral responses, which can be significantly adjusted using on-chip phase shifters. The distinguishing feature of our spectrometer lies in its inverse design approach, facilitating effortless control and efficient manipulation of the programmable circuit. By eliminating the need for intricate configuration, our design reduces power consumption and mitigates control complexity. Additionally, our reconfigurable spectrometer offers two distinct operating conditions. In the Ultra-High-Performance mode, it is activated by multiple phase-shifters and achieves exceptional spectral resolution in the picometer scale while maintaining broad bandwidth. On the other hand, the Ease-of-Use mode further simplifies the control logic and reduces power consumption by actuating a single-phase shifter. Although this mode provides a slightly degraded spectral resolution of approximately 0.3 nm, it prioritizes ease of use and is well-suited for applications where ultra-fine spectral reconstruction is not a primary requirement.

Keywords: silicon photonics; integrated spectrometers; computational spectrometers

Li A, Wu YF, Wang C et al. An inversely designed integrated spectrometer with reconfigurable performance and ultra-low power consumption. *Opto-Electron Adv* **7**, 240099 (2024).

Introduction

Integrated optical spectrometers have garnered significant interest due to their potential for integration into portable devices, enabling applications such as invasive food scanning, health monitoring, hyperspectral imaging and environmental sensing[1–3]. The key performance indicators include operation bandwidth, spectral resolution, dynamic range, power consumption and measurement period. The bandwidth refers to the optical range that the spectrometer can measure, while the spectral resolution is typically defined as the minimum interval between two peaks that can be distinguished from each other by the spectrometer. Frequently it is characterized by the narrowest bandwidth of a single peak resolved by the spectrometer. Typically the bandwidth and resolution are related and there exists tradeoff between them,

[1]National Key Laboratory of Microwave Photonics, Nanjing University of Aeronautics and Astronautics, Nanjing 210016, China; [2]Key Lab of Modern Optical Technologies of Education Ministry of China, Soochow University, Suzhou 215006, China; [3]College of Information Science and Electronic Engineering, Zhejiang University, Hangzhou 310058, China.

*Correspondence: ZY Yang, E-mail: yangzongyin@zju.edu.cn; SL Pan, E-mail: pans@nuaa.edu.cn

Received: 28 April 2024; Accepted: 3 June 2024; Published online: 17 July 2024

therefore, a new term named bandwidth/resolution ratio (BRR) can be used. The dynamic range is the difference between the maximum and the minimum optical intensity a spectrometer can handle. This is a system-level performance indicator that depends on various aspects including responsivity and noise floor of the photodetectors, maximum tolerable optical intensity in the waveguide, insertion loss (IL) of the spectrometer etc. For the interest of the spectrometer, it is the IL that matters most. Practical solutions suitable for real-life applications are still elusive due to performance limitations and impractical operating conditions, including high power consumption, long measurement periods, and complex control logic. Additionally, current demonstrations of integrated spectrometers only offer fixed performance, while reconfigurable performance is highly desirable for adjusting to dynamic and complicated working scenarios.

There are two broad categories of integrated spectrometers: passive spectrometers and scanning spectrometers. Passive spectrometers split incident light into multiple channels for parallel measurement using an array of detectors or imaging sensors, resulting in high hardware cost and low dynamic range[4–14], as plotted in Fig. 1(a). In contrast, scanning spectrometers using a single detector are more suitable for portable devices. They can be further classified into tunable-filter spectrometers, Fourier transform spectrometers (FTS), and switch-array-based spectrometers[15–23]. Tunable filter spectrometers measure the incident spectrum by sweeping a narrow peak of a tunable filter across the desired optical range, as illustrated in Fig. 1(b). The ultra-narrow linewidth of the filter leads to low intensity at the detector, compromising the dynamic range of the spectrometer[16,24]. Additionally, achieving broad bandwidth and high resolution will consume considerable amount of sweeping power and time, as evident by a recent study that necessitated 2501 sweeps to cover the 100 nm bandwidth, rendering it unfeasible for real-life applications[16]. Integrated FTS encounters similar challenges, as capturing the interferogram in the time domain consumes substantial power and time, which is shown in Fig. 1(c). Recent demonstrations have consumed hundreds of Watts and taken over an hour to obtain a complete interferogram[18,19,25].

An emerging architecture for scanning spectrometers is the switch-array-based spectrometer, which allows for the configuration of different physical channels using switches as plotted in Fig. 1(d). Researchers implemented an array of Mach-Zehnder Interferometer (MZI) switches to develop a digital FTS[21]. 64 discrete optical path delays (OPDs) by connecting different delay lines through the configuration of each switch are achieved. Similarly, a recent study implemented a switch array with 14 MZI switches to connect different microring resonators to formulate 256 physical channels with different spectral responses[22]. However, the use of multiple switches introduces the challenge of complex control logic, which poses difficulties for integrating these

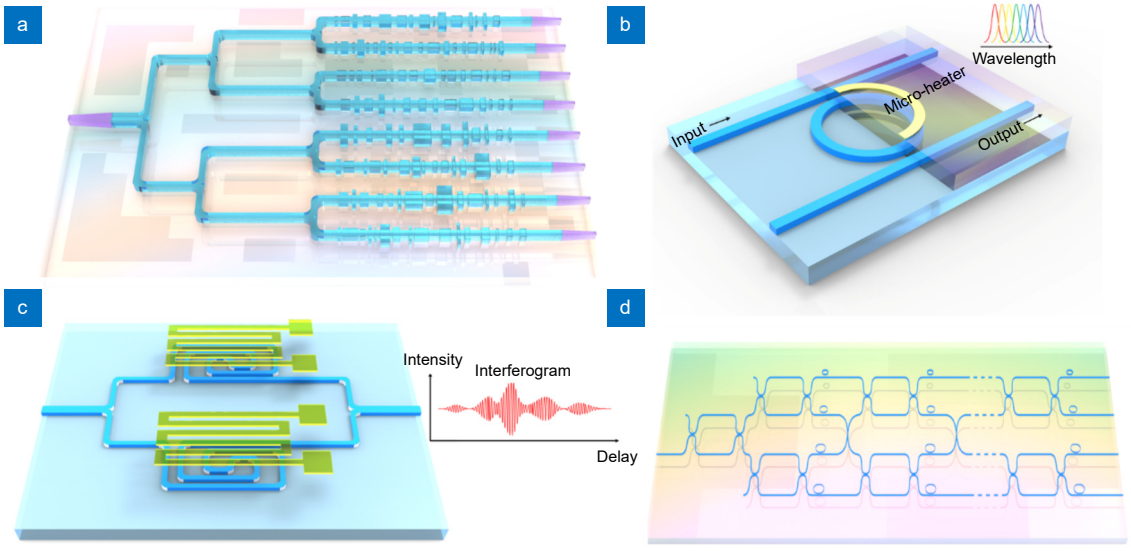

Fig. 1 | A few examples of different types of integrated spectrometers. (**a**) Passive spectrometer utilizing an array of stratified waveguide filters with distinct spectral responses. (**b**) Scanning spectrometer based on tunable narrowband filter, e.g. microring resonator. (**c**, **d**) Fourier transform spectrometer with continuous optical path delay enabled by thermo-optic effect (c) and switch-array to reconfigure the physical channels (d).

spectrometers into portable devices. Furthermore, achieving precise configuration between the cross and bar states for each MZI switch is crucial, but fabrication variations make it challenging to calibrate and determine the required power injection for correct switch configuration[26]. Moreover, the imperfections of integrated Mach-Zehnder Interferometer (MZI) switches, such as insertion loss, limited bandwidth, and low extinction ratio, impede scalability.

Table 1 summarizes the performance of different types of integrated spectrometers, the advantages are highlighted in red. This raises the question: Can we develop an integrated spectrometer that possesses the following characteristics so that it can be practically applied in real-life applications:

- broad bandwidth and high spectral resolution;
- high dynamic range, without multi-channel splitting and detector array;
- simple control logic, without precise monitoring and configuration of on-chip elements;
- low power consumption and a short measurement time;
- performance reconfigurability.

In this paper, our objective is to provide an answer to this question by demonstrating a user-friendly reconfigurable spectrometer on the silicon photonics platform, with the potential for mass fabrication at a low cost. The spectrometer utilizes pure waveguide elements with negligible losses, processing the entire spectrum simultaneously without any splitting elements and employs a single detector to collect all intensity, ensuring a large dynamic range. The design process of our spectrometer is reversed, allowing for the creation of a structure that can be easily controlled and manipulated by phase-shifters without the need for precise configuration. This simplifies operation, reduces power consumption, and eliminates the complexity associated with control systems. These advantages are particularly valuable for portable or battery-operated devices. Additionally, our spectrometer possesses a unique advantage in terms of reconfigurability, allowing it to switch between two distinct operating conditions:

1) Ultra-high performance mode: In this mode, the spectrometer is actuated by multiple phase shifters, enabling it to achieve an exceptional spectral resolution in the scale of picometers while maintaining a bandwidth of over 100 nm (limited by fiber/chip couplers). This high-resolution capability makes it well-suited for applications that require precise and detailed spectral analysis.

2) Ease of use mode: By actuating a single phase shifter at a time, the spectrometer operates in a mode that offers a slightly degraded spectral resolution of approximately 0.3 nm but with much lower power consumption and simplified control circuit. This configuration prioritizes ease of use and simplifies the overall operation of the spectrometer. It is particularly suitable for applications that do not necessitate ultra-fine spectral reconstruction but instead focus on factors such as device footprint, available power sources, and user convenience.

The ability to switch between these two operating conditions provides users with flexibility, making the spectrometer versatile and adaptable to a wide range of applications.

Principle

The core of our spectrometer is a programmable circuit, whose spectral responses can be programmed to distinct states $F_i(\lambda)$ (i=1, 2, 3,…,N) by applying electric signals into on-chip phase shifters. Each response $F_i(\lambda)$ is supposed to provide a sampling of the entire incident spectrum $\Phi(\lambda)$. The spectrum $\Phi(\lambda)$ can be reconstructed by post-processing the sampling results. Mathematically,

Table 1 | Performance summary of different types of integrated spectrometers.

	Passive[9]	Scanning spectrometers			Ideal
		Tunable filter[16]	Fourier transform[19]	Switch-array based[21]	
BRR	1000	2500	1125	100	>1000
Insertion loss (w/o coupling loss)	~20 dB	>30 dB	~15 dB	~10 dB	<2 dB
Number of detectors	64	1	3	1	1
Control complexity	Simple	Complex	Complex	Complex	Simple
Power consumption	No	85 mW	3 W	99 mW	<100 mW
Time consumption	Picosecond	Millisecond	Hours	Millisecond	Millisecond
Reconfigurability	No	No	No	Yes	Yes

when a signal with optical spectrum of $\Phi(\lambda)$ passes through a physical channel with spectral response of $F(\lambda)$ and gets absorbed by a detector, the generated electrical signal will be $I=\int_{\lambda_1}^{\lambda_M}\Phi(\lambda)F(\lambda)\,\mathrm{d}\lambda$, where λ_1, λ_M is the starting and ending wavelength of the spectrum, respectively. The equation can also be re-written in the discrete way as $I=\sum_{i=1}^{i=M}\Phi(\lambda_i)F(\lambda_i)=\Phi_{1\times M}F_{M\times 1}$. Then employing N different spectral responses will generate N electrical signals, expressed by following equation:

$$\boldsymbol{I}_{1\times N}=\boldsymbol{\Phi}_{1\times M}\boldsymbol{F}_{M\times N}\,. \tag{1}$$

This is N linear equations, with M unknowns $(\Phi_1\cdots\Phi_M)$ representing the incident spectrum. The equations can still be solved with adequate accuracy even when the number of equations is much smaller than the number of unknowns ($N<<M$), as long as the channels' spectral responses have sufficient randomness and low cross-correlation. Under this condition, the system is under-determined and should be solved by solving following equation:

$$\begin{aligned}&\text{minimize}\left|\,|\boldsymbol{I}_{1\times N}-R\boldsymbol{\Phi}_{1\times M}\boldsymbol{F}_{M\times N}|\,\right|^2\\&+\alpha\,||\,\boldsymbol{\Gamma}\boldsymbol{\Phi}^{\mathrm{T}}{}_{1\times M}||^2,\\&\text{subject to } 0\le\boldsymbol{\Phi}_{1\times M}\le 1\,,\end{aligned} \tag{2}$$

where $||\cdots||^2$ means the Euclidean norm, α is a factor determining the regularization strength and $\boldsymbol{\Gamma}$ is an auxiliary matrix to modify $\boldsymbol{\Phi}_{1\times M}$ for regularization. In previous demonstrations, an array of broadband filters with different structural parameters was utilized to generate

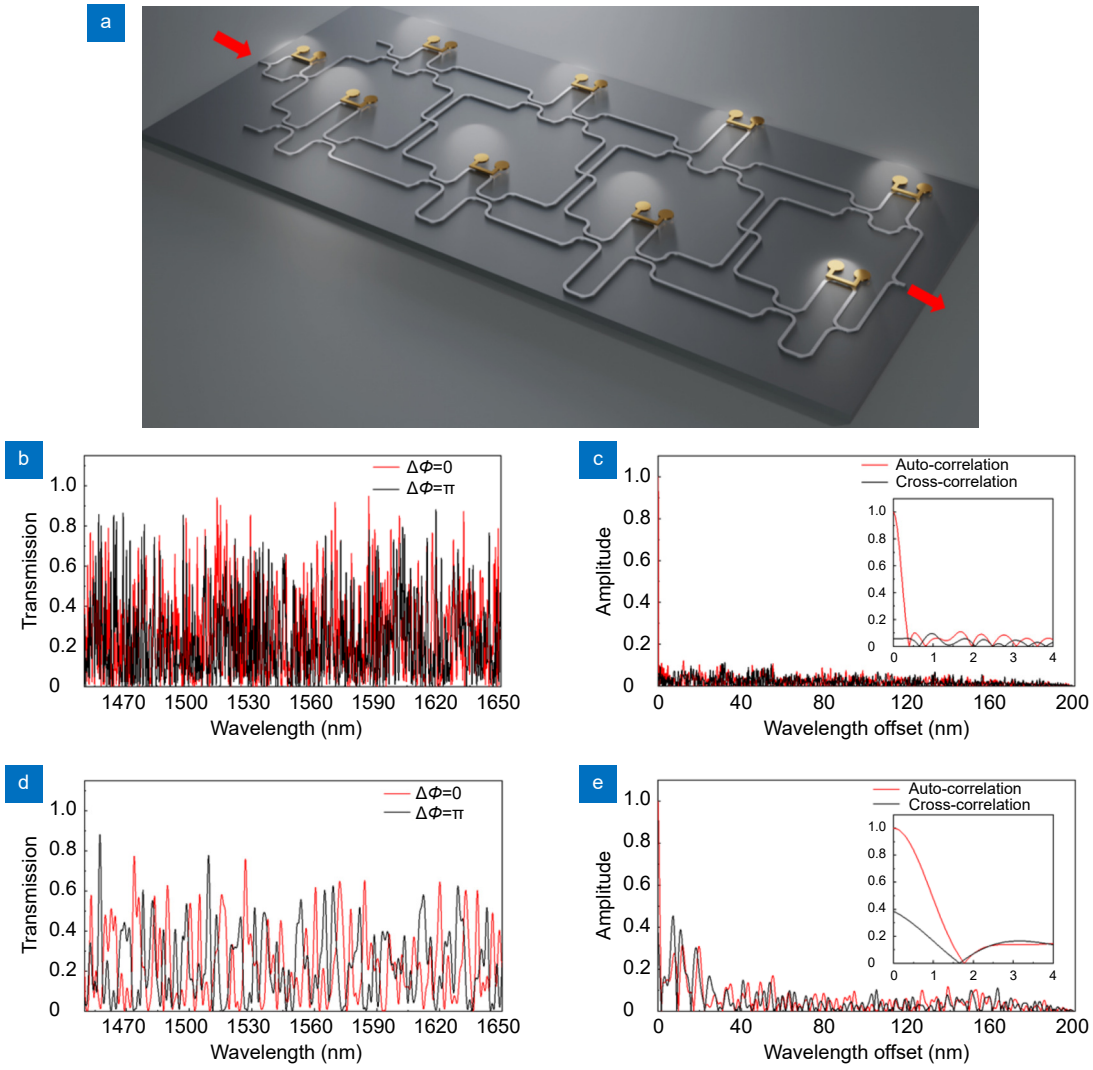

Fig. 2 | (**a**) Structure of our proposed programmable circuit. (**b**) Simulated spectral responses for the inversely designed structure with 0 and π phase changes applied to the 11 phase shifters, respectively. (**c**) Auto-correlation and cross-correlations of the spectral responses of the inversely designed circuit. (**d**) Simulated spectral responses for the randomly designed structure with 0 and π phase changes applied to the 11 phase shifters, respectively. (**e**) Auto-correlation and cross-correlations of the spectral responses of the randomly designed circuit.

distinct spectral responses. However, this approach often required more than 30 filters, resulting in over 15 dB of additional loss[9–12,27]. Consequently, the intensities of the detected signals were low, and the signal-to-noise ratio (SNR) was compromised. Moreover, this approach makes the spectrometer produce a fixed performance, which can not be used for dynamic working scenarios.

In contrast, our developed programmable structure employs a single-input-single-output configuration, where the spectral responses can be programmed to distinct conditions by applying electrical signals. As a result, there is no need for physical splitting, leading to a substantial improvement in dynamic range. Compared to other scanning spectrometers, our device eliminates the need for complex and precise control over multiple phase shifters. Instead, power injections can be randomly chosen to enable dramatic changes in the structure's spectral responses. This flexibility in power injection enables the spectrometer to achieve different configurations without requiring intricate control systems. This user-friendly characteristic sets it apart from other spectrometers and simplifies its operation. Our spectrometer also offers the flexibility to reconfigure its performance and control logic based on the specific application requirements. It can operate in two distinct states: ultra-high performance mode and ease of use mode.

Inverse design of the programmable spectrometer

Programmable photonic circuits have been extensively studied and applied in various fields, but mainly limited to signal processing[28,29]. In this work, we propose to utilize a simplified programmable photonic circuit for spectra reconstruction. The structure of the programmable circuit, as shown in Fig. 2(a), consists of a 2D array of imbalanced Mach-Zehnder Interferometers (iMZIs) interconnected in a mesh configuration. This arrangement creates a complex interference pattern through multiple pathways between the input and output, resulting in a randomized spectral response. The spectral characteristics of the circuit can be modified by adjusting the working conditions of each iMZI through power injection into the phase shifters, depicted in gold in the figure. The iMZIs in the structure are characterized by their arm length (L), length imbalance (ΔL), and coupling coefficient (κ), which serve as the structural parameters. The design of this structure aims to achieve a static spectral response with high spectral resolution, which means we're suppressing the full-wave-half-maximum (FWHM) of the auto-correlation of the spectral response. Additionally, it seeks to maximize sensitivity to changes in the working conditions of the iMZIs, thereby minimizing the power consumption required to modify the spectral responses. Traditional approaches to designing such a structure with N iMZIs would involve optimizing $3N$ structural parameters, which is a challenging and time-consuming task. Applying intelligent inverse design on integrated optics has been extensively studied for optimized performance[30]. Among various inverse design algorithms, we propose utilizing particle swarm optimization (PSO) for the inverse optimization of these structural parameters due to its fast convergence rate and excellent ability for global optimization searching[31–36].

For a given iteration of the PSO algorithm, a figure of merit (FoM) is utilized to determine the quality of current iteration. In our case, the objective is to minimize the auto-correlation (AC) of the spectrum, thus to produce high sampling resolution. Additionally, we are targeting a structure that is very sensitive to phase change in the arms of the iMZIs. To account for both effects, the final FoM is determined as follows:

$$FoM = \sqrt{\sum_{j=1}^{j=M} AC_1^{\,2}(\lambda_j)} + \alpha \frac{1}{\sqrt{\sum_{j=1}^{j=M} \left(F_1(\lambda_j) - F_2(\lambda_j)\right)^2}}. \tag{3}$$

The first term represents the AC of the spectral responses, minimizing the AC allows us to design a spectrometer with higher spectral resolution. The second term captures the sensitivity of the spectral response to a unit phase change in each iMZI within the structure, where $F_1(\lambda)$ and $F_2(\lambda)$ refer to the original spectral response and the modified spectral response when a phase change of π is introduced to the arm of each iMZI. To balance the importance of these two terms, we include an adjustment factor α in the FoM. Note that, there are multiple waveguide crossings in this structure, and they are also inversely optimized using PSO for high transmission efficiency.

Simulations of programmable circuit

We use aforementioned procedure to inversely design a programmable spectrometer consisting of 11 iMZIs. Each iMZI incorporates a phase shifter to modify its working condition. We use an in-house optical circuit simulator to perform the simulations of the circuit's

spectral responses under different working conditions of those iMZIs. First of all, we'd like to demonstrate the value of inverse design by comparing two structures: one randomly designed and the other designed using inverse design with PSO algorithm. Specifically, we analyze the spectral responses when the 11 phase shifters receive 0 phase change and π phase changes, respectively. Figure 2(b–e) showcases the results of this comparison. It reveals that utilizing inverse design leads to significant improvements in the spectrometer's performance. Firstly, there is a remarkable 6 times reduction in the full-width-half-maximum (FWHM) of the auto-correlations. A reduced FWHM indicates enhanced spectral resolution, which is a crucial factor in spectrometer performance. Additionally, the cross-correlations between the two spectral responses are reduced by over 4 times when inverse design is employed. Lower cross-correlations signify a decrease in interference and better isolation between the spectral responses, further enhancing the accuracy and reliability of the spectrometer.

Next, we proceed with the simulated behavior of the inversely designed structure. When actuating all 11 phase shifters simultaneously, the spectral responses from 1450 nm to 1650 nm exhibit clear randomness and distinction as depicted in Fig. 3(a), confirming the broad bandwidth of our circuit. Notably, the 11 phase shifters were configured randomly and the phase changes are all within π as illustrated in Fig. 3(b), which plots the phase changes implemented in each phase shifter. This emphasizes the high-sensitivity and ease-of-use of our spectrometer. Furthermore, the auto-correlations presented in Fig. 3(c) demonstrate the ultra-high spectral resolution as the FWHM of each auto-correlation peak is less than 0.2 nm. To assess the linear dependency between the spectral responses, we examined the cross-correlations, as illustrated in Fig. 3(d). The cross-correlations remained below 0.3 across the 200 nm span, indicating very low linear dependency.

The 11 phase shifters can be randomly actuated to drive the spectrometer, which already simplifies the control compared to previous approaches that require more phase shifters and precise configurations. However, the spectrometer can be further simplified to actuate only one phase shifter at a time with the rest phase shifters remains inactivated. As evident in Fig. 3(e–f), the spectral responses of the programmable circuit can also be notably changed when actuating just one phase shifter of any iMZI at a time. Even if the auto-correlations and cross-correlations become degraded compared with previous case as shown in Fig. 3(g–h), but still, the multiple distinct spectral responses produced by the programmable circuit can be used for stochastic sampling of the incident spectrum. In applications where ultra-high performance is not essential, the ability to operate with a single phase shifter significantly simplifies the control scheme and reduces complexity.

In summary, by providing the flexibility to choose between ultra-high performance and simplified control, the spectrometer becomes a valuable tool that can address different needs and priorities. In applications where precision and high performance are critical, driving all 11 phase shifters allows for fine-grained control and optimal spectral resolution. On the other hand, in scenarios where control simplicity and ease of use are paramount, driving just a single phase shifter offers a simplified approach. This expands its potential areas of use and makes it a valuable tool for applications that prioritize flexibility and control ease.

Results and discussion

The chip is sent for fabrication at Applied Nanotools. The structures were defined on a 220 nm thick silicon-on-insulator wafer using E-beam lithography with high fabrication accuracy, with feature size reported to be less than 60 μm. The structure layer is sitting on top of a 2 μm thick buried oxide layer to prevent leakage to the 725 μm handle wafer and is covered by a 3 μm thick oxide cladding layer for protection. The patterning process begins by cleaning and spin-coating a material that is sensitive to electron beam exposure. A device pattern is defined into this material using 100 keV EBL. Once the material has been chemically developed, an anisotropic ICP-RIE etching process is performed on the substrate to transfer the pattern into the underlying silicon layer. The microscopic image of the fabricated structures and photograph of the packaged chip is given in Fig. 4(a). Vertical grating couplers are used as fiber-chip coupling elements and they are inversely designed to ensure 3 dB bandwidth over 80 nm. We use a programmable 64-channel power supply to actuate the on-chip phase shifters. 400 spectral responses of the programmable spectrometer under different working conditions of the phase shifters are measured using tunable laser source, covering span from 1460 nm to 1580 nm (Agilent 8164B system). Each phase shifter's power injection is between 0 and 15 mW to ensure max π phase change, as the P_π of

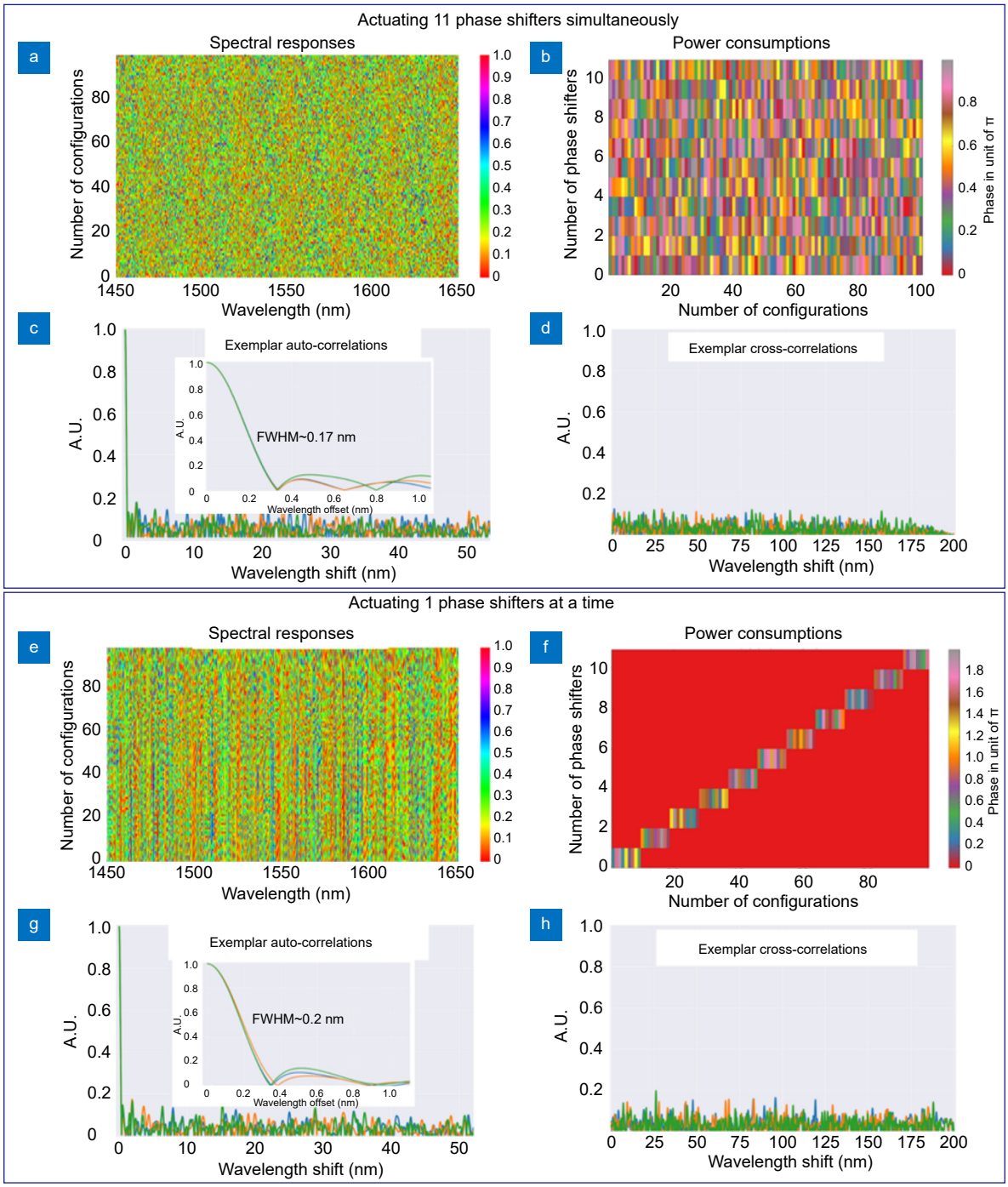

Fig. 3 | (**a–d**) Simulations when actuating 11 phase shifters simultaneously. (a) Simulated spectral responses under 100 different configurations of 11 phase shifters. (b) Phase changes of the 11 phase shifters. (c) Exemplar auto-correlations of those spectral responses. (d) Exemplar cross-correlations between several spectral responses. (**e–h**) Simulations when actuating single phase shifter at a time. (e) Simulated spectral responses under 100 different configurations of all 11 phase shifters. (f) Phase changes of the 11 phase shifters. (g) Exemplar auto-correlations of those spectral responses. (h) Exemplar cross-correlations between several spectral responses.

our phase shifter is measured to be around 13 mW. The raw data of the 400 spectral responses are plotted in Fig. 4(b) and the corresponding power consumptions of phase shifters are given in Fig. 4(c). The transmissions between 1460 nm and 1475 nm are very low as they are sitting at the edge of the grating couplers' bandwidth. Some exemplar auto-correlations and the cross-correlations of the 400 responses are given in Fig. 4(d, e), respectively. As expected, by injecting random amounts of power into 11 phase shifters, the spectral responses of the

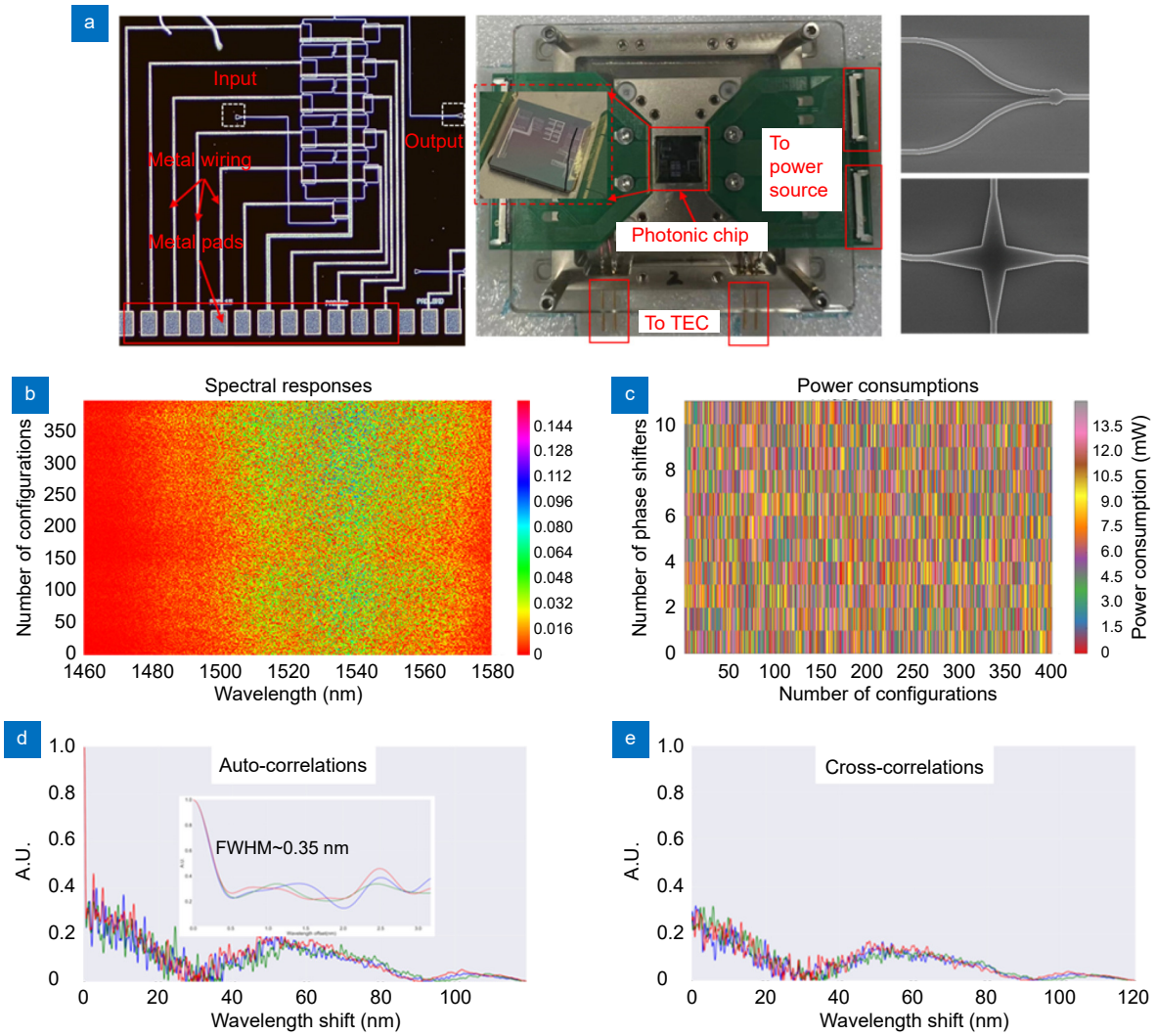

Fig. 4 | (**a**) Images of the fabricated chip. (**b–e**) Experimental results when actuating 11 phase shifters simultaneously. (b) Spectral responses under 400 different configurations of 11 phase shifters. (c) Power consumptions of the 11 phase shifters. (d) Exemplar auto-correlations of those spectral responses. (e) Exemplar cross-correlations between several spectral responses.

circuit can be programmed to very distinct shapes, which are suitable for stochastic and independent sampling of the incident unknown spectrum. The FWHMs of the auto-correlations are in good consistency with simulations, which are around 0.35 nm, confirming very high spectral resolution. The levels of cross-correlations are higher than simulations, due to parasitic effects that add additional correlations to spectral responses, such as the fiber facet reflections etc. Similar to other silicon photonics devices, fabrication variation would impact the designed spectral responses from its target. However, we believe for our structure, the fabrication variation is not a big concern, as the structure only consists of simple elements such as waveguides and directional coupler and all the sub-components have been verified multiple times in standard MPW run. Besides, the minimum structure feature size (namely the gap of the directional couplers) is ensured to be larger than 180 nm, which can be guaranteed by current CMOS technology. Also for the computational spectrometer, it is not the actual spectral response that matters, as long as the spectral response is sufficiently random with narrow FWHM of the autocorrelation, the device should work.

We also test the ability to work with actuating single phase shifter at a time. 2.5 mW difference in the power consumption to one phase shifter can already produce visible difference to the spectral responses, as evident in Fig. 5(a). Therefore, the power consumption to any one phase shifter is swept between 0 and 30 mW with 2.5 mW increment, in total 132 spectral responses of the

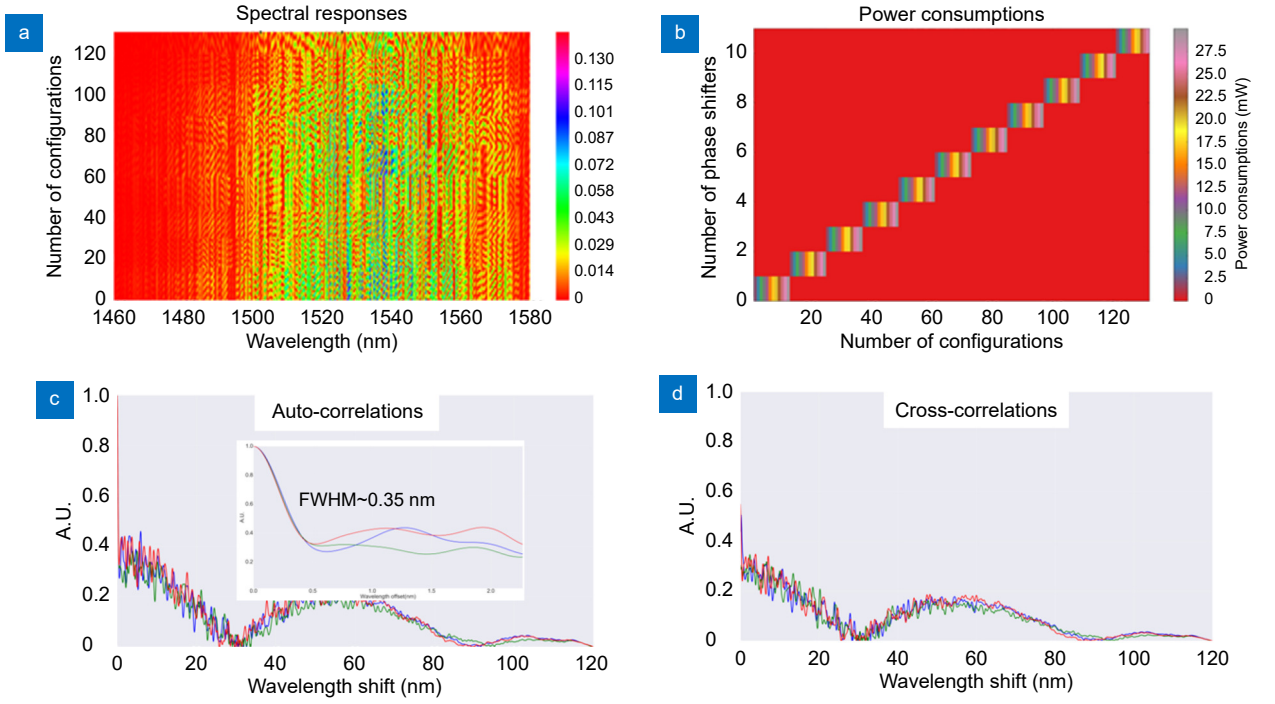

Fig. 5 | Experimental results when actuating 1 phase shifters at a time. (**a**) Spectral responses under 132 different configurations of all 11 phase shifters. (**b**) Power consumptions of the 11 phase shifters. (**c**) Exemplar auto-correlations of those spectral responses. (**d**) Exemplar cross-correlations between several spectral responses.

programmable spectrometer by actuating only one phase shifter at a time are generated and plotted in Fig. 5(b). The corresponding power consumptions of those phase shifters are shown in Fig. 5(c). The auto-correlations and the cross-correlations of the responses are given in Fig. 5(d, e), respectively. Naturally, we notice a slight degradation in the cross-correlations compared with the case when actuating all 11 phase shifters simultaneously.

Next, a various of spectra were sent to our programmable spectrometer for reconstruction. The reconstructions were achieved using CVX program in MATLAB to solve the under-determined problem. First, we sent narrow peaks with MHz linewidth at different wavelengths from our laser source to the spectrometer to test the resolution. The reconstructions at two working modes (by actuating 11 phase shifters and 1 phase shifter) are given in Fig. 6(a, b), respectively. The FWHMs of the reconstructed peaks are around 6 pm and 150 pm for two modes. To further test the spectral resolution, we send spectrum consisting of two closely standing peaks for reconstruction. When working at mode 1, the minimum distance between two peaks that can be clearly resolved is 10 pm, while for mode 2, it is 300 pm. A broadband spectrum from a ASE source is also sent for test. Both working modes can reconstruct the spectrum with very high accuracy, but mode 1 still produces a higher accuracy. Besides those simple spectra that are either sparse or smooth, we also take the challenge of reconstructing a complex dense spectrum that consists of mostly non-zero spectral components with 3 narrow notches. The spectrum is generated by sending a broadband SLD spectrum (3 dB bandwidth ~110 nm) to 3 cascaded Fiber Bragg gratings (FBGs) with varying bandwidths (0.1 nm, 0.1 nm and 0.2 nm) and center wavelengths (1549.5 nm, 1550 nm, 1550.5 nm), followed by an optical bandpass filter with 15 nm bandwidth (Yenista XTM50). Due to the large number of distinct spectral responses generated at mode 1, the complex dense spectrum can also be accurately reconstructed. Even at mode 2, we notice a nice overall reconstruction, but with greater discrepancy. To provide comparisons with existing integrated spectrometers, the key performance indicators of several exemplary works are listed in Table 2. Clearly, our spectrometer maintains broad bandwidth and high spectral resolution with unique feature of low insertion loss, low power-consumption, simple control logic and reconfigurability.

Conclusions

We have developed an inversely-designed, user-friendly

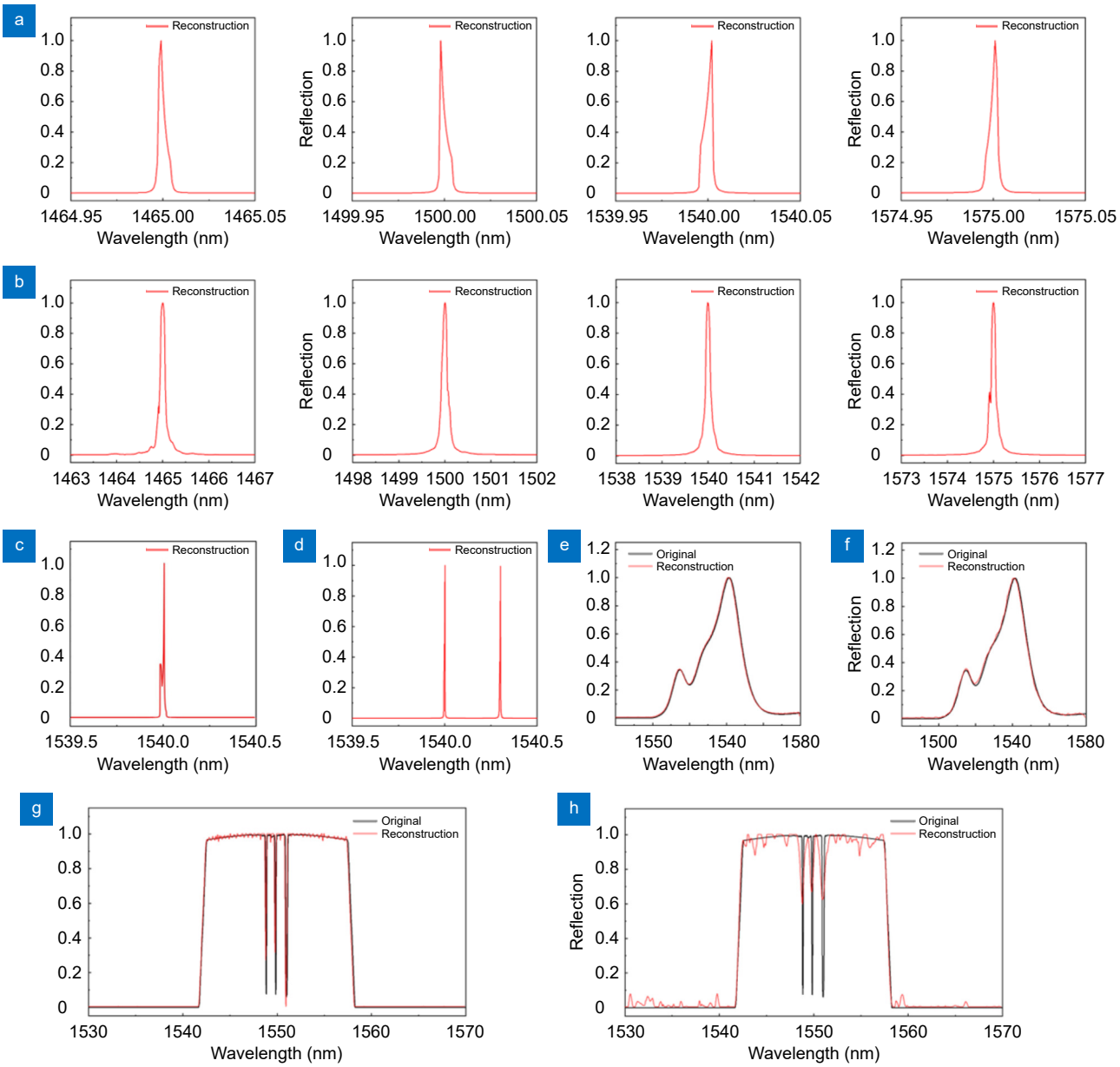

Fig. 6 | Reconstructions of various narrow peaks when the spectrometer working at mode 1 (a) and mode 2 (b), with a resolution of 6 pm and 150 pm, respectively. Reconstructions of two closely standing narrow peaks when the spectrometer working at mode 1 (**c**) and mode 2 (**d**), with a minimum distance of 15 pm and 300 pm, respectively. Reconstructions of broad spectrum when the spectrometer working at mode 1 (**e**) and mode 2 (**f**). Reconstructions of a complex dense spectrum when the spectrometer working at mode 1 (**g**) and mode 2 (**h**).

integrated spectrometer that operates with reconfigurable performance. It is based on a programmable photonic circuit, whose spectral responses can be notably modified using electrical signals. The design process is reversed, allowing for the creation of a structure that can be easily controlled and manipulated by a single phase-shifter. This innovative design addresses the challenges faced by traditional spectrometers, offering improved efficiency and ease of use. It can operate in two distinct modes: ultra-high performance mode by actuating 11 phase shifters or ease-of-use mode by actuating only one phase shifter. The first mode can produce a bandwidth of 120 nm and a spectral resolution at the scale of pm. The second mode can produce the same bandwidth but with a poorer resolution of 0.3 nm. But with a single phase-shifter and minimal power requirements, the need for complex and power-consuming control systems is eliminated. This is a significant advantage, particularly for portable or battery-operated devices, where power consumption is a critical factor.

Table 2 | Comparisons of our work with existing integrated spectrometers.

	Category	BRR	IL (dB)	No. of detectors	Control logic	Power consumption	Size (mm^2)
ref.[8]	Passive	20	20	20	N/A	N/A	9
ref.[9]		1000	20	64	N/A	N/A	4
ref.[16]	Scanning	2500	30	1	Complex	85	0.0036
ref.[19]		1125	15	3	Complex	3000	>4
ref.[21]		100	10	1	Complex	99	N/A
Our		10,000@mode 1 333@mode 2	<1	1	Simple	120@mode 1 30@mode 2	0.5

Overall, our inversely-designed, user-friendly integrated spectrometer offers a compelling solution for various applications, combining efficient operation, low power consumption, and ease of use.

References

1. Yang ZY, Albrow-Owen T, Cai WW et al. Miniaturization of optical spectrometers. *Science* **371**, eabe0722 (2021).
2. Li A, Yao CH, Xia JF et al. Advances in cost-effective integrated spectrometers. *Light Sci Appl* **11**, 174 (2022).
3. Chen C, Li XY, Yang G et al. Computational hyperspectral devices based on quasi-random metasurface supercells. *Nanoscale* **15**, 8854–8862 (2023).
4. Seyringer D, Sagmeister M, Maese-Novo A et al. Compact and high-resolution 256-channel silicon nitride based AWG-spectrometer for OCT on a chip. In *2019 21st International Conference on Transparent Optical Networks (ICTON)* 1–4 (IEEE, 2019); http://doi.org/10.1109/ICTON.2019.8840473.
5. Gatkine P, Veilleux S, Hu YW et al. Arrayed waveguide grating spectrometers for astronomical applications: new results. *Opt Express* **25**, 17918–17935 (2017).
6. Xia ZX, Eftekhar AA, Soltani M et al. High resolution on-chip spectroscopy based on miniaturized microdonut resonators. *Opt Express* **19**, 12356–12364 (2011).
7. Redding B, Liew SF, Sarma R et al. Compact spectrometer based on a disordered photonic chip. *Nat Photonics* **7**, 746–751 (2013).
8. Ma KQ, Chen KX, Zhu N et al. High-resolution compact on-chip spectrometer based on an echelle grating with densely packed waveguide array. *IEEE Photonics J* **11**, 4900107 (2019).
9. Li A, Wang C, Bao FX et al. An integrated single-shot spectrometer with large bandwidth-resolution ratio and wide operation temperature range. *PhotoniX* **4**, 29 (2023).
10. Li A, Fainman Y. On-chip spectrometers using stratified waveguide filters. *Nat Commun* **12**, 2704 (2021).
11. Wang Z, Yi S, Chen A et al. Single-shot on-chip spectral sensors based on photonic crystal slabs. *Nat Commun* **10**, 1020 (2019).
12. Redding B, Liew SF, Bromberg Y et al. Evanescently coupled multimode spiral spectrometer. *Optica* **3**, 956–962 (2016).
13. Gao H, Fan XH, Wang YX et al. Multi-foci metalens for spectra and polarization ellipticity recognition and reconstruction. *Opto-Electron Sci* **2**, 220026 (2023).
14. Zheng ZH, Zhu SK, Chen Y et al. Towards integrated mode-division demultiplexing spectrometer by deep learning. *Opto-Electron Sci* **1**, 220012 (2022).
15. Dong P, Qian W, Liang H et al. Thermally tunable silicon racetrack resonators with ultralow tuning power. *Opt Express* **18**, 20298–20304 (2010).
16. Xu HN, Qin Y, Hu GL et al. Breaking the resolution-bandwidth limit of chip-scale spectrometry by harnessing a dispersion-engineered photonic molecule. *Light Sci Appl* **12**, 64 (2023).
17. Sun CL, Chen ZQ, Ye YT et al. Scalable on - chip microdisk resonator spectrometer. *Laser Photonics Rev* **17**, 2200792 (2023).
18. Souza MCMM, Grieco A, Frateschi NC et al. Fourier transform spectrometer on silicon with thermo-optic non-linearity and dispersion correction. *Nat Commun* **9**, 665 (2018).
19. Li A, Fainman Y. Integrated silicon fourier transform spectrometer with broad bandwidth and ultra-high resolution. *Laser Photonics Rev* **15**, 2000358 (2021).
20. Zheng SN, Zou J, Cai H et al. Microring resonator-assisted Fourier transform spectrometer with enhanced resolution and large bandwidth in single chip solution. *Nat Commun* **10**, 2349 (2019).
21. Kita DM, Miranda B, Favela D et al. High-performance and scalable on-chip digital Fourier transform spectroscopy. *Nat Commun* **9**, 4405 (2018).
22. Yao CH, Chen MJ, Yan T et al. Broadband picometer-scale resolution on-chip spectrometer with reconfigurable photonics. *Light Sci Appl* **12**, 156 (2023).
23. Zhang L, Zhang M, Chen TN et al. Ultrahigh-resolution on-chip spectrometer with silicon photonic resonators. *Opto-Electron Adv* **5**, 210100 (2022).
24. Krishna RM, Eftekhar A, Lee S et al. Polysilicon micro-heaters for resonance tuning in CMOS photonics. *Opt Lett* **47**, 1097–1100 (2022).
25. Xu HN, Qin Y, Hu GL et al. Scalable integrated two-dimensional Fourier-transform spectrometry. *Nat Commun* **15**, 436 (2024).
26. Li K, Yang M, Cai CK et al. Handling mode and polarization in fiber by fs-laser inscribed (de)multiplexer and silicon switch array. *PhotoniX* **4**, 14 (2023).
27. Gao L, Qu YR, Wang LH et al. Computational spectrometers enabled by nanophotonics and deep learning. *Nanophotonics* **11**, 2507–2529 (2022).
28. Bogaerts W, Pérez D, Capmany J et al. Programmable photonic circuits. *Nature* **586**, 207–216 (2020).
29. Xie YW, Hong SH, Yan H et al. Low-loss chip-scale programmable silicon photonic processor. *Opto-Electron Adv* **6**, 220030 (2023).
30. Wang N, Yan W, Qu YR et al. Intelligent designs in nanophotonics: from optimization towards inverse creation. *PhotoniX* **2**, 22 (2021).
31. Zagaglia L, Floris F, O'Brien PA. Experimental characterization

of particle swarm optimized focusing non-uniform grating coupler for multiple SOI thicknesses. *J Lightwave Technol* **39**, 5028–5034 (2021).

32. Fu PH, Chao CY, Huang DW. Ultracompact silicon waveguide bends designed using a particle swarm optimization algorithm. *IEEE Photonics J* **13**, 6600509 (2021).
33. Chen WW, Li HX, Zhang BH et al. Silicon mode (de) multiplexer based on cascaded particle-swarm-optimized counter-tapered couplers. *IEEE Photonics J* **13**, 6600210 (2021).
34. Mak JCC, Sideris C, Jeong J et al. Binary particle swarm optimized 2× 2 power splitters in a standard foundry silicon photonic platform. *Opt Lett* **41**, 3868–3871 (2016).
35. Abedi K, Mirjalili SM. Slow light performance enhancement of Bragg slot photonic crystal waveguide with particle swarm optimization algorithm. *Opt Commun* **339**, 7–13 (2015).
36. Djavid M, Mirtaheri SA, Abrishamian MS. Photonic crystal notch-filter design using particle swarm optimization theory and finite-difference time-domain analysis. *J Opt Soc Am B* **26**, 849–853 (2009).

Acknowledgements

We are grateful for financial supports from following sources: National Key R&D Program of China (grant No. 2021YFB2801500) National Natural Science Foundation of China (grant No. 62375126, No. 62105149 and No. 62334001) Natural Science Foundation of Jiangsu Province (grant No. BK20210288) Opening Foundation of Key Laboratory of Laser & Infrared System (Shandong University), Minister of Education Key Lab of Modern Optical Technologies of Education Ministry of China, Soochow University State Key Laboratory of Advanced Optical Communication Systems and Networks, China Specially-appointed Professor Fund of Jiangsu.

Author contributions

A. Li and Z. Y. Yang conceived the idea. Y. F. Wu, C. Wang and F. X. Bao performed the simulations, device design and layout generation. A. Li and Y. F. Wu performed the measurements. A. Li, Y. F. Wu and Z. Y. Yang analysed the data and prepared display items. S. L. Pan supervised the projects. All authors contributed to and reviewed the manuscript.

Competing interests

The authors declare no competing financial interests.

Scan for Article PDF